Neural mechanisms of handedness for precision drawing: hand-dependent engagement of cortical networks for bimanual control and tool use

Kapil N[1]*, Kim T[1,2]*, Gassass S[1], Zhou R[3], Carter AR[4], Dobbins IG[5], Liu L[3], McAvoy MP[1], Wheelock MD[6], Wang Y[7], Brogan DM[8], Dy CJ[8], Mackinnon SE[9], Philip BA[1]

*: Co-first authors

1: Program in Occupational Therapy, Washington University School of Medicine, St. Louis MO
2: Kinesiology, Physical Medicine & Rehabilitation, Pennsylvania State University, University Park PA
3: Biostatistics, Washington University School of Medicine, St. Louis MO
4: Neurology, Washington University School of Medicine, St. Louis MO
5: Psychological & Brain Sciences, Washington University, St. Louis MO
6: Radiology, Washington University School of Medicine, St. Louis MO
7: Obstetrics & Gynecology, Washington University School of Medicine, St. Louis MO
8: Orthopedic Surgery, Washington University School of Medicine, St. Louis MO
9: Plastic & Reconstructive Surgery, Washington University School of Medicine, St. Louis MO

Corresponding author: Benjamin Philip, benjamin.a.philip@gmail.com

Conflict of interest statement: Author BAP has a licensing agreement with PlatformSTL to commercialize a version of the drawing task used in this work.

Funding statement: This work was supported by NINDS R01 NS114046 to BAP.

Data availability statement: The data that support the findings of this study will be made openly available upon completion of clinical trial NCT05207878.

ABSTRACT

The neural mechanisms of handedness remain poorly understood, particularly for lateralized movements such as precision drawing. Using functional magnetic resonance imaging (fMRI), we examined how healthy adults and individuals with peripheral nerve injury (PNI) in their dominant hand performed a visually guided drawing task with each hand. We hypothesized that the left superior parietal lobule (SPL) supports drawing with either hand, and that individuals with PNI would recruit the same mechanisms as healthy adults.

Methods: 33 Right-handed adults (23 healthy adults, 10 patients) underwent fMRI while performing a precision drawing task, alternating between the right hand (RH) and left hand (LH). LH>RH effects were examined across 20 regions of interest (12 a priori, 8 post hoc) using two approaches: (1) BOLD magnitude, and (2) functional connectivity (FC) modulation, assessed via generalized psychophysiological interaction.

Results: All effects describe LH drawing > RH drawing. Right primary motor cortex (M1) had lower magnitude and greater FC with two networks, both of which exhibited equal-or-greater magnitude: a left hemisphere M1-dorsal premotor circuit, and an intrahemispheric parieto-temporal circuit. Right M1 (also had reduced interhemispheric FC with inferior parietal lobule, which exhibited lower magnitude. Patient group had no effect on magnitude or FC.

Conclusions: Three neural mechanisms differentiate LH from RH drawing in right handed adults. First, a left hemisphere system for bimanual control, which engages intrahemispherically (directly) during RH drawing but interhemispherically (indirectly) during LH drawing. Second, LH drawing increases engagement of a contralateral system that may reflect increased task demands. Third, RH drawing increases engagement of an interhemispheric circuit for tool use. The first and third systems may explain performance asymmetries associated with handedness. Patients with PNI use the same mechanisms as healthy adults, highlighting these mechanisms' potential as a neuromodulatory target to enhance LH performance after RH impairment.

INTRODUCTION

Little is known about the neural mechanisms of left-right asymmetries in upper limb performance ("performance asymmetries" for brevity), even though these performance asymmetries are a fundamental aspect of everyday human behavior. Human handedness is a multifactorial concept(Dexheimer et al., 2024), one aspect of which is performance asymmetries. These asymmetries arise from lateralized cortical specializations for different aspects of movement. According to the complementary dominance theory(Kitchen et al., 2025; Britne A Shabbott & Robert L Sainburg, 2008), in right-handed individuals, the left hemisphere contains specializations for precision control of trajectories and multi-joint synergies, while the right hemisphere contains specializations for impedance and stabilization. Each of these lateralized specializations supports bilateral action, but is primarily connected to the contralateral hand, leading to e.g. a right-hand (RH) advantage for smooth trajectories. However, these neural specializations cannot yet be assessed or targeted to support rehabilitation because the specific neural mechanisms of performance asymmetries remain unknown.

Our current understanding of the neural mechanisms underlying performance asymmetries is based on lesion and neuroimaging studies, each of which offer different limitations. Lesion studies have shown that the left hemisphere contains a specialization that supports precision trajectory control with both hands, consistent across two-dimensional reaching tasks with complex demands (Schaefer et al., 2012) and simpler tasks such as ballistic two-dimensional reaching (Mani et al., 2013; Schaefer et al., 2009) or finger-tapping sequences (Haaland et al., 2004). However, lesion studies cannot provide anatomical precision due to lesion heterogeneity, nor can they distinguish between stroke-related deficits and post-stroke adaptation. Neuroimaging allows precise spatial measurement, but is often restricted to even simpler movements: such studies have identified a role for left M1 in bilateral finger tapping (Hayashi et al., 2008; Tzourio-Mazoyer et al., 2015), increased involvement of ipsilateral M1 under high task demands during two-finger joystick movements (Barany et al., 2020; Buetefisch et al., 2014; Wischnewski et al., 2016), and greater interhemispheric functional connectivity (FC) for the non-preferred hand (NPH) vs. PH during simple open/close fist movements (Tsurugizawa et al., 2023). Overall, few neuroimaging tasks capture the precision trajectory control that defines the PH's performance advantage (see previous paragraph), let alone the mechanisms involved in real-world upper limb actions.

Real-world movements—such as writing, using utensils, or reaching in cluttered environments—involve a dynamic integration of feedforward and feedback mechanisms (Kringelbach et al., 2023; Peterson et al., 2021). Investigating the neural basis of these real-world processes necessitates ecologically valid tasks that capture the complexity and variability of natural behavior rather than artificially constrained experimental conditions (Finn et al., 2020, 2022). This recognition has prompted a growing shift in cognitive neuroscience toward naturalistic functional MRI (fMRI) designs that incorporate dynamic stimuli such as movies, narratives, and virtual reality (Bottenhorn et al., 2019; Saarimäki, 2021; Zhang et al., 2021). These approaches elicit rich, multimodal brain activity and engage distributed neural networks, including regions that remain unrecruited during simpler tasks, leading to deeper insights into real-world cognition (Hasson et al., 2010). Despite the challenges of applying naturalistic paradigms to motor function (Scarapicchia et al., 2017)(Reddy et al., 2023), naturalistic motor tasks such as real-time visual feedback (Karimpoor et al., 2018; Yang et al., 2024) and reaching and grasping of 3D objects (Freud et al., 2018) can elicit distinct activation patterns. These findings support the need for demanding and ecologically-relevant motor paradigms in fMRI studies to better understand the neural basis of lateralized motor control.

The neural mechanisms of handedness hold critical clinical relevance to patients with chronic impairment of the PH. Chronic PH impairment occurs frequently despite surgery and/or rehabilitation, affecting approximately 22% of hemiplegic stroke patients and 22% of patients with upper extremity peripheral nerve injury (PNI). Better outcomes following PH-PNI are associated with improved performance of the NPH (Kim et al., 2024), but strategies to facilitate NPH use during rehabilitation remain poorly understood (Philip Jove & Marcori et al., 2019). Bridging this gap requires a mechanistic understanding of the asymmetric neural mechanisms of naturalistic action. To that end, we developed a fMRI visually-guided precision drawing task (Philip & Frey, 2014; Philip et al., 2023) designed to engage participants in an ecologically relevant activity (control of a pen) that requires both feedforward and feedback control during continuous dynamic movements. Critically, pen control skills have a strong PH advantage in most humans(Blank et al., 2000), and therefore are uniquely impaired in patients with chronic impairment of the PH (Philip et al. 2017). By having participants perform this task with their PH and NPH, we aim to isolate the mechanisms that support PH-like action in the NPH – mechanisms that could be targeted to enhance rehabilitation outcomes in individuals with chronic PH deficits.

In the current study, we isolated "PH-like action with the NPH" (in right-handed participants, thus "RH-like action with the LH") via a task fMRI study of participants while they performed a precision drawing task with each hand (LH and RH, separately). We analyzed blood oxygenation level dependent (BOLD) magnitude via general linear models (GLM), and functional connectivity (FC) via generalized psychophysiological interactions (gPPI). Based on previous work (Philip et. al, 2021), we hypothesized that precision drawing's LH > RH difference ($hand_{LH-RH}$) would entail greater ipsilateral BOLD magnitude in a superior parietal lobule (SPL) locus. In addition, to establish the neural correlates for the processes of adapting to chronic PH impairment after neurological injury, we hypothesized that patients with chronic PNI to the PH would use the same neural mechanisms as healthy adults.

METHODS

Participants

Thirty-three right-handed adults (24 female; ages 47 ± 18, range 24-82) performed a visually-guided precision drawing task (see *fMRI Task* below) in the fMRI scanner. 10/33 participants had peripheral nerve injuries (PNI) to their right arm ("patients"). Participant demographics are listed in **Table 1** and their clinical characteristics are listed in **Table 2**. Two additional patients were excluded from the current analysis because they were unable to complete the task with their affected RH, and four additional participants were excluded due to poor task compliance or excess motion, as detailed below (see *Motion Correction and Screening* below); these excluded participants are not included in the n=33. All participants gave informed consent, and all procedures were approved by the Institutional Review Board at Washington University in St. Louis School of Medicine.

Sample size was based on a power analysis using preliminary data (N=26)(Kim et al., 2023), which showed potential positive $hand_{LH-RH}$ effects (i.e. LH > RH) in BOLD magnitude in one region of interest (ROI): superior parietal lobule ipsilateral to movement, SPL-ipsi; see *ROI Selection* below) (Mumford, 2012). We performed a simulation-based power analysis via a linear mixed model with a random intercept for each subject. The model included behavioral covariates (velocity and direction, separately for each hand or as a difference or ratio) and demographic confounds (sex, age, group). Sample size estimation was conducted via a bootstrap procedure with 500 bootstrap resampled datasets. The analysis indicated that a sample size of N=30 would achieve 90% power at a two sided significance level

of $\alpha = 0.05$. To accomodate potential participant exclusion we increased the target sample size to N=39, o after screening (see led to 33 participants.

Characteristic	Total (n=33)	Patient (n=10)	Controls (n=23)	Between groups
Age (y), mean ± SD	48 ± 18	52 ± 17	46 ± 18	t = -0.818, p = 0.424
Sex (female), n (%)	24 (74%)	7 (73%)	17 (74%)	$\chi^2 = 0.00$, p = 1.000
Race/Ethnicity, n				Fisher: df = 6, p = 0.900
Native American	1	1	0	
White	22	7	15	
Black	5	1	4	
Asian	3	1	2	
Hispanic and/or Latino	1	0	1	
Middle Eastern/North African	1	0	1	
Prefer not to say	1	0	1	
Education, n				Fischer: df = 2, p = 1.000
High school or equivalent	2	0	2	
Some college	20	7	13	
Post college degree (e.g., Masters)	10	3	7	

Table 1. Demographic characteristics. Between-group differences were assessed with independent-sample t tests (continuous data), chi-square (χ^2) tests (categorical data), or Fisher's exact test (multi-category data). All participants had at least a high school education.

Clinical Characteristics	Patient (n=10)
Severity, n	
Neurapraxia	6
Axonotmesis	3
Neurotmesis	2
# Surgeries (for this injury)	0.91 ± 0.83
Time since last surgery (mo)	7.60 ± 12.88
Time since injury (mo)	9.55 ± 11.94
Affected nerve, n	
Ulnar	6
Median	5
Radial	2
Other	3
Injury location, n	
Brachial Plexus	2
Elbow	2
Forearm	2
Wrist	7
Hand	2
Nerve transfer surgery = Yes	2 (18%)

Table 2. Patients' clinical characteristics. Totals may not add to 10 due to multiple injuries/nerves/locations per patient.

fMRI Acquisitions

Scans were performed on a Siemens PRISMA 3T MRI scanner. fMRI BOLD EPIs were collected using a T2*-weighted gradient echo sequence, a standard 64-channel birdcage radio-frequency coil, and the following parameters: TR = 662 ms, TE = 30 ms, flip angle = 52°, 72 x 72 voxel matrix, FOV = 216 mm, 60 contiguous axial slices acquired in interleaved order, resolution: 3.0 x 3.0 x 3.0 mm, bandwidth = 2670 Hz/pixel, multi-band acceleration = 6x. Siemens auto-align was run at the start of each session. High-resolution T1-weighted structural images were also acquired, using the 3D MP-RAGE pulse sequence: TR = 4500 ms, TE = 3.16 ms, TI = 1000 ms, flip angle = 8.0°, 256 x 256 voxel matrix, FOV = 256 mm, 176 contiguous axial slices, resolution: 1.0 x 1.0 x 1.0 mm. A T2-weighted image was also acquired at: TR = 3000 ms, TE = 409 ms, 256 x 256 voxel matrix, FOV = 256 mm, 176 contiguous axial slices, resolution: 1.0 x 1.0 x 1.0 mm. Spin echo field maps were also collected before the functional runs.

fMRI Task

Each participant completed six BOLD functional scans while performing a visually guided precision darwing task based the STEGA app (Philip & Frey, 2014; Philip et al., 2023). The task was performed using one hand per scan, alternating between left and right hand across the six scans (three scans per hand). During the task, participants saw hollow shapes, and were instructed to draw a line within the bounds of the shape, as fast as possible while prioritizing staying in-bounds over speed. To minimize head and shoulder motion, participants were also instructed to draw by moving their fingers and hand, while keeping their upper arm and forearm as still as possible. Participants were provided with a real-time visual feedback through a video overlay of their (transparent) hand/pen over the drawn shape, using an MRI-compatible drawing tablet with bluescreen technology (Karimpoor et al., 2015; Tam et al., 2011), as shown in **Figure 1**. Pen position data was collected at 60 Hz. The task was presented in a block design with 15.2 seconds (23 images) of drawing, followed by 15.2 seconds (23 images) of rest (fixation cross). A scan comprised ten cycles of draw/rest, with an additional rest block at the start, and 3.3 seconds (5 images) of additional rest after the final rest block, leading to a total duration of 5:23 (488 volumes total: 230 drawing, 258 rest) per scan. Immediately prior to the scan, participants completed 1 block with each hand in a mock fMRI scanner to familiarize with the task, apparatus, and drawing while keeping their arm still.

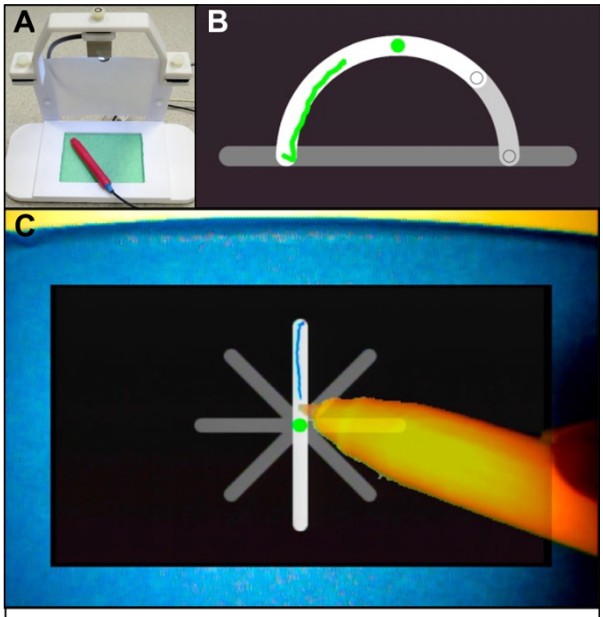

Figure 1. Motor task used for pipeline testing. A: MRI-compatible tablet. B: STEGA precision drawing task. C: Participant view of bluescreen integration.

fMRI Preprocessing. The data were preprocessed using *fMRIPrep* 24.1.1(Esteban et al., 2019; RRID:SCR_016216), which is based on *Nipype* 1.8.6(Gorgolewski et al., 2011; RRID:SCR_002502). Many internal operations of *fMRIPrep* use *Nilearn* 0.10.4 (Abraham et al., 2014; RRID:SCR_001362), mostly within the functional processing workflow.

Anatomical preprocessing*:* The T1-weighted (T1w) volume was corrected for intensity non-uniformity with N4BiasFieldCorrection(Tustison et al., 2010), distributed with ANTs 2.5.3(Avants et al., 2008; RRID:SCR_004757). The T1w-image was skull-stripped using antsBrainExtraction.sh workflow (using

OASIS30ANTs template). The segmentation of cerebrospinal fluid (CSF), white-matter (WM) and gray-matter (GM) was performed on the brain-extracted T1w using fast (FSL, RRID:SCR_002823,(FSL, Zhang et al., 2002; RRID:SCR_002823). Brain surfaces were reconstructed using recon-all (FreeSurfer 7.3.2, Dale et al., 1999; RRID:SCR_001847), and the brain mask was refined by reconciling ANTs- and FreeSurfer-derived segmentations of the cortical gray-matter of Mindboggle(Klein et al., 2017; RRID:SCR_002438). Finally, the T1w volume was normalized to symmetrical MNI standard space (*ICBM 152 Nonlinear Symmetrical template version 2009c* [RRID:SCR_008796; TemplateFlow ID: MNI152NLin2009cSym]) using nonlinear registration with antsRegistration (ANTs 2.5.3), producing an anatomical reference for functional co-registration.

Functional preprocessing: Each of the six BOLD functional runs was motion-corrected by estimating rigid-body transformations to a reference volume using mcflirt(FSL, Jenkinson et al., 2002). The estimated *fieldmap* was then aligned with rigid-registration to the target EPI (echo-planar imaging) reference run. The field coefficients were mapped on to the reference EPI using the transform. The BOLD reference was then co-registered to the T1w reference using bbregister(Freesurfer, Greve & Fischl, 2009). Several confounding time-series were calculated based on the *preprocessed BOLD*: framewise displacement (FD) along with the WM, CSF, and global signal. FD was computed using fsl_motion_outliers (relative root mean square displacement between affines, Jenkinson et al., 2002)). The WM and CSF signals were extracted from masks derived from the brain segmentations, and the global signal from the whole brain mask. Three global signals were extracted from CSF, the WM, and the whole-brain masks. Additionally, a set of physiological regressors were extracted to allow for component-based noise correction (CompCor, Behzadi et al., 2007). Principal components were estimated after high-pass filtering the *preprocessed BOLD* time-series (using a discrete cosine filter with 128s cut-off) for the two *CompCor* variants: temporal (tCompCor) and anatomical (aCompCor). tCompCor components were then calculated from the top 2% variable voxels within the brain mask. For aCompCor, three probabilistic masks (CSF, WM and combined CSF+WM) were generated in anatomical space. These masks were resampled into BOLD space and binarized by thresholding at 0.99. The head-motion estimates and CSF, WM, and global signals were expanded with the inclusion of temporal derivatives and quadratic terms for each(Satterthwaite et al., 2013). Additional nuisance timeseries were calculated by means of principal components analysis of the signal found within a thin band (*crown*) of voxels around the edge of the brain, as proposed by Patriat et al. (2017). All resamplings were performed with *a single interpolation step* by composing all the pertinent transformations (i.e. head-motion transform matrices, susceptibility distortion correction when available, and co-registrations to anatomical and output spaces). Gridded (volumetric) resamplings were performed using nitransforms, configured with cubic B-spline interpolation.

fMRI Motion Outlier Identification and Screening

Three methods were used to identify and exclude participants based on motion, task-correlated motion, or poor task compliance. These methods excluded 4 participants in total; these 4 are not counted in the n=33 sample size.

To identify participants with high motion, we employed two criteria: 1) Participant-level FD threshold: Head motion was quantified using FD, computed at each volume and summarized across runs for each participant. 36 of initial 37 screened participants had FD < 0.5 mm, a commonly used cutoff for large head motion; the single participant exceeding 0.5 mm was excluded. This participant also exhibited pen-contact errors, reinforcing the exclusion; 2) Volume-wise motion outliers: We identified high-motion volumes using FSL_motion_outliers (Jenkinson et al., 2012) to identify volumes within each scan with FD > an outlier threshold of 75th percentile + (1.5 * inter-quartile range). This threshold identified 4.6% of

volumes as outliers (# outlier volumes per scan: range 0-68, mean 22.4, quartiles 10, 20, 33). A participant would be removed from analysis due to excess motion if their # outliers exceeded 20% of the data (98 volumes) in any scan, but no participants met that threshold.

Participants were screened for excess task-correlated motion by quantifying the coefficient of determination (Pearson r^2) between FD and the task timecourse. Correlation was calculated for each run, and averaged across runs within each participant. These values ranged 0-0.075 (mean 0.020, median 0.017). This process was repeated for the first derivative of the task timecourse, leading to correlation values that ranged 0-0.144 (mean 0.044, median 0.031). Participants were excluded from analysis if their correlation value exceeded the outlier threshold of 75th percentile + (1.5 * inter-quartile range) for either the timecourse (threshold $r^2 = 0.161$) or its derivative (threshold $r^2 = 0.239$). Based on this screening, 2 participants were removed from analysis.

To identify participants who failed to comply with the task, a two-step process was used. First, experimenters qualitatively evaluated participant compliance during data collection (a yes/no warning flag); 7 participants were flagged for follow-up. Second, the flagged participants were explored using objective data for 3 measures of task compliance: number of finger touches (which cause the drawn line to jump across the screen), amount of time spent drawing during drawing blocks (which would be low if the participant was slow to notice the change from rest to draw), and performance (BIS, see *Behavioral Data Analysis* below). One flagged participant had the highest number of touches of all participants, and also had the 3rd-lowest performance, so this participant was excluded from analysis. No other participants showed atypical task compliance, though 3/7 flagged participants had been excluded due to excessive head motion and task-correlated motion as described above. The remaining 3/7 flagged participants did not show atypical task compliance by any objective metric and thus were retained in the sample.

Performance Analysis

Pen position was recorded at 60 Hz during drawing blocks of the fMRI task. To remove artifacts caused by the participant accidentally touching the tablet with a finger (which caused the recorded location to "jump" instantly across the tablet), raw data points were removed if their velocity (mm/sec) exceeded the 4th standard deviation, calculated within each scan. All analyses were performed in MATLAB 24.2.0 (Mathworks, Natick MA).

Based on the position data, six performance measures were calculated: position accuracy ("posErr" for brevity; -1 * position error, mm), smoothness "velSm" ("velSm;" -1 * number of velocity peaks per 45 mm shape part), direction accuracy "dirAcc" ("dirAcc;" -1 * direction error, degrees), velocity ("spd" to avoid confusion with velSm; root mean squared, mm / s), and two secondary measures: Balanced Integrated Score (BIS, "bis") and Speed Accuracy Tradeoff (SAT, "sat"), detailed in the following paragraphs.

BIS captures overall performance by integrating speed and accuracy measures(Liesefeld & Janczyk, 2023; Vandierendonck, 2021). BIS is calculated for each participant-hand pair (i.e. each participant had a LH and a RH value) as zscore(speed) + zscore(position accuracy), using participant-hand averages for speed and error, and z-scoring across the entire dataset (all participants & hands). An alternative calculation of BIS was explored using direction accuracy rather than position accuracy, but the two measures were highly correlated ($r^2 > 0.9$), so only position accuracy was used.

SAT captures participant tradeoffs between fast (feedforward) and slow corrective (feedback) actions, to assess the participant's relative reliance on the two lateralized components in the dynamic dominance hypothesis: the left-hemisphere feedforward specialization and right-hemisphere feedback

specialization(Sainburg, 2002; Wang & Sainburg, 2007). Following our calculation of BIS, we determined SAT as zscore(speed) – zscore(position accuracy), such that a high SAT values will reflect a fast imprecise movement.

Performance variables were initially generated at the participant-hand level, but for each participant the LH and RH values were highly colinear, reflecting the existence of a "bilateral/overall dexterity" participant trait (**Table 3** column 1). To enable analysis of left/right performance differences without collinearity, an "asymmetry" value ("Asym") was calculated for each participant and variable as (RH-LH)/(RH+LH) (after offset to minimum=0), such that high values represent the advantage of the preferred RH(Vingerhoets et al., 2023). Asymmetry's correlations with LH and RH were uniformly lower than the correlation between LH and RH, as shown in **Table 3** columns 2-3.

The "bilateral/overall dexterity" trait also manifested as across-variable correlations (**Supplementary Table 1**), which were addressed by avoiding collinearities via the 3-step model creation process described below (*ROI Analysis*).

Therefore, the final set of performance variables included 18: the six measures (position accuracy, smoothness, direction accuracy, velocity, BIS, SAT), each with separate values for LH, RH, and Asym.

	Coefficient of determination (r^2)		
Variable	**LH : RH**	**Asym : LH**	**Asym : RH**
Position Accuracy	0.357	0.038	0.427
Smoothness	0.829	0.009	0.228
Direction Accuracy	0.564	0.101	0.148
Velocity	0.856	0.003	0.101
SAT	0.865	0.000	0.112
BIS	0.826	0.036	0.048

Table 3. Coefficients of determination (r^2) between performance variables across hands and asymmetry indices.

fMRI Analyses

The task fMRI data were analyzed to identify where BOLD magnitude and/or FC were stronger for LH drawing than RH drawing ($hand_{LH-RH}$). In summary, our fMRI data analysis entailed 6 steps: First, data were reoriented into "ipsilateral/contralateral" (to movement) hemispheres. Second, a *priori* regions of interest (apROIs) were selected. Third, magnitude was analyzed via a GLM analysis performed with FSL 6.0.7.12 (FMRIB, Oxford UK)(Smith et al., 2004). Fourth, to identify behavioral factors associated with BOLD magnitude, each ROI was analyzed with a generalized linear mixed effects model (GLME). Fifth, to identify additional regions with $hand_{LH-RH}$ effects on BOLD magnitude, exploratory whole-brain analyses were performed. Sixth, $hand_{LH-RH}$ modulation of FC was identified via generalized psychophysiological interaction (gPPI) (McLaren et al., 2012), performed with CONN 22.v2407 (Nieto-Castanon, 2020).

Data Reorientation: To allow direct comparison of LH vs. RH movement, the data (after motion outlier identification and fMRIprep preprocessing, including registration to symmetric template MNI152NLin2009cSym) from RH runs were left-right flipped. This produced images where the left side of the image consistently represented the hemisphere ipsilateral to movement, and the right side the hemisphere contralateral to movement. Thereafter, all data were analyzed as "ipsilateral/contralateral" to movement.

Region of Interest (ROI) selection: Twelve apROIs were chosen, six areas in each hemisphere (ipsilateral "-ipsi" and contralateral "-contra" to movement). The six areas were selected based on previous work implicating their role in lateralized control of precision hand movement: M1, IPS, 7A, SPL, PMd, and SMA. Each ROI was a 4 mm radius sphere determined from the following prior studies: The M1 seed was based on normative sensorimotor hand area (Philip & Frey, 2014). The IPS seed was chosen as the voxel with peak activation from left hemisphere areas that previously showed interhemispheric changes related to learning—specifically, where training-related increases in FC with right M1 correlated with NPH skill learning (Philip & Frey, 2016; fig. 4a). The 7A seed was chosen from the left hemisphere areas that previously showed interhemispheric changes related to learning and retention—specifically, where training-related changes in FC with right M1 predicted long-term retention of NPH skill(Philip & Frey, 2016; fig. 5a); for this ROI, the seed was selected as the first local maximum with >50% odds of being in cortex (which was also the local maximum with the greatest odds of being inside the brain, 78%) instead of the voxel of peak activation, because the peak was on the cortical surface (-34, -54, 67) and would have produced an ROI substantially outside the brain. The SPL seed was chosen as the voxel with peak activation from right hemisphere areas that previously showed convergent interhemispheric changes that predicted future learning–specifically, where pre-training FC from both left M1 and left IPS correlated with subsequent NPH learning (Philip et al., 2021; fig. 4). The PMd seed was chosen as the voxel with peak drawing-specific magnitude in left PMd (Philip et al., 2021; Potgieser et al., 2015). The SMA seed was chosen as the voxel with peak activation during a hand movement task that previously identified SMA as having a primary role in effective connectivity underpinning lateralized performance(Pool et al., 2014). Spheres were limited to the volume whose chance of being in the appropriate anatomical area according to the Juelich Histological Atlas (Eickhoff et al., 2006; Eickhoff et al., 2007) exceeded a cutoff; the cutoff for parietal and SMA ROIs was ≥ 25%, and PMd was ≥10% because its peak voxel only had a 21% chance of being in Brodmann's Area 6. However, these anatomical cutoffs did not lead to the removal of any voxels. When necessary, seeds from prior studies were transformed to the symmetric template MNI152NLin2009cSym (Fonov et al., 2009) via FLIRT before sphere creation. The ROI seed coordinates in the MNI152NLin2009cSym template were as follows: M1 (±40, −24, 56), IPS (±52, −42, 44), 7A (±20, −62, 68), SPL (±34, −58, 46), PMd (±26, −8, 52), and SMA (±6, −6, 56).

Magnitude analysis (GLM): The reoriented data were integrated from fMRIprep tor FSL using established workarounds (Mumford, 2017), followed by spatial smoothing with a 6 mm FWHM SUSAN filter and high pass temporal filtering with 60 sec cutoff; no other preprocessing was applied via FSL. Explanatory variables (EVs) were modeled, along with their temporal derivatives, according to the block design described in the previous section (*fMRI Task*), with additional confound EVs based on head motion parameters (3 variables each for translation and rotation) and motion outliers calculated as described above. The hemodynamic response was accounted for by convolving the model with a double-gamma function. Run-level contrasts of parameter estimates (COPEs) were calculated for Task vs. Rest. The run-level COPEs (Task > Rest) were averaged across runs using a fixed-effects model to produce participant-level results, which were used for the ROI analyses detailed in the next section.

In addition, the signal to noise ratio (SNR) was calculated for each participant as σ (Task>Rest) / σ (model) (Masharipov et al., 2024b), averaged across runs.

ROI Analysis: To identify factors that influenced BOLD magnitude in each ROI, a three-step process was performed: univariate factor testing, model design, and a multivariate generalized linear mixed effects model (GLME). 22 candidate factors were used: the 18 performance variables described above (6 measures * LH, RH, Asym), age, sex (labeled "sexF" to indicate positive effects for female), group

(patient, control), and drawing hand ("$hand_{LH-RH}$," i.e. LH-drawing > RH-drawing). $Hand_{LH-RH}$ was always included in the final GLME to address our study hypotheses, and therefore was ignored in factor testing and treated differently in model design.

In the first step (factor testing), a univariate t-value was produced for each candidate factor in each ROI. BOLD magnitude was modeled using a univariate general linear model (GLM), separately for each ROI, based on each candidate factor (except for handLH, which did not need testing because it was automatically included in the final model). This resulted in 504 univariate GLMs (12 apROIs * 21 factors). Note that to achieve a univariate design, BOLD was measured separately for each drawing hand (e.g. separate models for BOLD-M1-ipsi-$hand_{LH}$ vs. BOLD-M1-ipsi-$hand_{RH}$) because some factors were measured at the participant level and were thus identical during the $hand_{LH}$ and $hand_{RH}$ conditions.

In the second step (model design), a multivariate model was built for each ROI using the most-relevant factors while avoiding collinearity. Specifically, the model for each area was built using the following process: Each area's model started with the factor "$hand_{LH-RH}$" to test the study hypothesis, and the random effect variable "subject" to address the repeated measures structure (2 values per participant, $hand_{LH}$ and $hand_{RH}$). Then, each other candidate factor was evaluated in order from highest to lowest absolute *t* value (from univariate analysis): if the new factor was not correlated with any previously evaluated factors (Pearson's *r*, α = 0.05/# of tests), the new factor was added to the model. This process produced 6-8 factors per model: subject, hand, and 4-6 other candidate factors.

In the third step (multivariate GLME), BOLD magnitude in each ROI was modeled using a GLME via the MATLAB function 'fitglme,' with factors determined by the model design step. GLME was selected because BOLD magnitudes were normally distributed across participants. To assess statistical significance of each model vs. chance, the likelihood ratio test (MATLAB 'compare') was used. "Chance" was determined via a bootstrap method. In each draw, factor values were randomly permuted across participants, independently for each factor; and a p-value was calculated using the likelihood ratio test. Reported p-values represent the average across 500 draws.

No multiple comparison correction was applied because the study was powered to detect effects in our primary hypothesized region, SPL-ipsi (see power analysis in *Participants* above). However, because effects were found in ROIs other than SPL-ipsi, the study's sensitivity to the observed effects was evaluated via simulation-based sensitivity (post-hoc power) assessment (Green et al., 2016). For each ROI, subjects were resampled with replacement (preserving all within-subject observations) and the full GLME was refit using the same factors as above. This process was repeated 500 times across a range of total sample sizes, and power was estimated power as the proportion of simulations in which the $hand_{LH-RH}$ effect was statistically significant at $\alpha = 0.05$. Importantly, this analysis quantifies the study's sensitivity to the effect sizes actually observed**,** rather than claiming an achieved power, consistent with current recommendations to avoid retrospective power reporting .

Exploratory whole-brain analysis: Group-level analyses were performed by averaging across participants, and modeling EVs for each participant (to capture the repeated-measures structure of LH vs. RH data for each participant), as well one EV of interest. For the primary analysis, the EV of interest was $hand_{LH-RH}$, which had the value +1 for LH data and –1 for RH data. Secondary analyses were performed with alternate EVs of interest: (1) group, (2) $hand_{LH-RH}$ * group interaction, and (3) $hand_{LH-RH}$ * confound interaction, for each confound strong enough to be included in any of our ROI analysis models (see *ROI Analysis* above, "model design" step). During all group-level analyses, Z-statistic images were created using cluster thresholding at $Z > 3.1$, $p < 0.05$.

To identify areas with $hand_{LH-RH}$ effects outside our apROIs, the significant clusters in the group-level analysis of $hand_{LH-RH}$ were used to determine post hoc ROIs (phROIs). The following process was used: If the cluster overlapped with any apROI, it was omitted. The cluster was assigned to an anatomical area based on highest-weight assignment in the Harvard–Oxford cortical or subcortical atlas (Caviness Jr et al., 1996; Desikan et al., 2006; Seidman et al., 1999); if two clusters shared an assignment, correlation was assessbed between the clusters' timecourses; and if significantly correlated, the lower-zscore cluster was omitted. For all remaining clusters, the center of gravity (and its homolog in the opposite hemisphere) was used as the seed for new bilateral phROIs, which were created and analyzed via the procedures described in the previous two sections. Note that for each bilateral pair of post hoc ROIs, GLME analysis of one hemisphere is statistically invalid due to double-dipping (Kriegeskorte et al., 2009), but both hemispheres are reported for comparison and quantification.

Functional Connectivity (FC) & Generalized Psychophysiological Interaction (gPPI) analysis: To idenfify hand-dependent ($hand_{LH-RH}$) modulation of FC, a gPPI analysis was performed in the CONN toolbox (22.v2407). First, the reoriented data were smoothed using spatial convolution with a Gaussian kernel of 6 mm FWHM; no other preprocessing was applied via CONN. Denoising was performed using the standard CONN pipeline (Nieto-Castanon, 2020), which included regressing out confounding signals from white matter and CSF BOLD signals (five components each), based on the anatomical component-based noise correction method (aCompCor) (Behzadi et al., 2007) along with six realignment parameters and their first derivatives, outlier scans, condition effects and their first-order derivatives, and linear detrending. High-pass filtering was subsequently applied to retain signal fluctuations above 0.008 Hz.

ROI-to-ROI functional connectivity between the twelve apROIs was evaluated via gPPI. For each seed–target ROI pair, the first-level model included three predictors: (i) HRF-convolved psychological regressors for condition (drawRH, drawLH, and rest); (ii) the physiological regressor (the seed ROI BOLD time series); and (iii) condition-specific interaction terms (PPI) formed by multiplying (i) and (ii), indexing modulation of connectivity between the ROIs. For each connection, the condition-dependent change in connectivity was defined as the bivariate regression coefficient (β) for the corresponding PPI term. At the second level, PPI β's were analyzed with connection-wise random-effects GLMs across participants to test task effects; the primary contrast was drawLH > drawRH (i.e. $hand_{LH-RH}$). Multiple comparisons were controlled using CONN's parametric, connection-based framework with Benjamini–Hochberg FDR across connections; significance was set at FDR-corrected $p < 0.05$.

To contextualize gPPI's connectivity-modulation values with a measurement of actual connectivity, standard ROI-to-ROI FC (not gPPI) was estimated separately for LH > rest and RH > rest (Agren et al., 2024).

To prevent phROIs from influencing our multiple comparison correction, the above analyses were first performed for apROIs only, followed by a second analysis including both the apROIs and phROIs. Note that FC analysis of phROIs is not double-dipping, because the ROIs were defined based on BOLD magnitude data.

RESULTS

We found that, during LH execution of a visually guided precision drawing task (vs. RH), M1 contralateral to movement showed lower BOLD magnitude, and greater functional connectivity (FC) with two networks: M1/PMd ipsilateral to movement, and a contralateral parietotemporal network, which generally had greater BOLD magnitude during LH drawing – except for ipsilateral PMd, where BOLD magnitude was effector-independent.

Drawing with the LH involves higher BOLD magnitude in ipsilateral frontal motor and contralateral parietal areas

We identified whether BOLD magnitude varied with drawing hand (i.e. $hand_{LH-RH}$) in our 12 apROIs (6 areas * 2 hemispheres, ipsilateral and contralateral to movement). In each ROI, we modeled BOLD signal magnitude with a GLME that included $hand_{LH-RH}$ and the strongest non-colinear performance/confound factors (for on each factor's univariate strength in each ROI see **Supplementary Tables 2-3**).

Multiple bilateral cortical areas were sensitive to $hand_{LH-RH}$, with significant effects in bilateral M1, SPL, IPS, and SMA (except that SPL-contra was a non-significant trend, p = 0.06), as visualized and quantified in **Figure 2a**, with full model details in **Supplementary Table 4**. Notably, frontal motor areas M1 and SMA showed a positive effect of $hand_{LH-RH}$ (i.e. LH>RH) in the ipsilateral hemisphere, and negative (RH>LH) in the contralateral hemisphere. The reverse pattern appeared in parietal areas SPL and IPS, which showed a negative effect of $hand_{LH-RH}$ (RH>LH) in the ipsilateral hemisphere, and positive (LH>RH) in the contralateral hemisphere. In other words, drawing with the LH (vs. RH) led to greater ipsilateral BOLD magnitude in frontal motor areas, but greater contralateral BOLD magnitude in parietal areas.

Performance-related effects appeared in M1-contra only (*p* 0.01-0.04; all others p ≥ 0.054), as expected because the current design was powered to detect effects of the factor $hand_{LH-RH}$, not quantitative effects of performance.

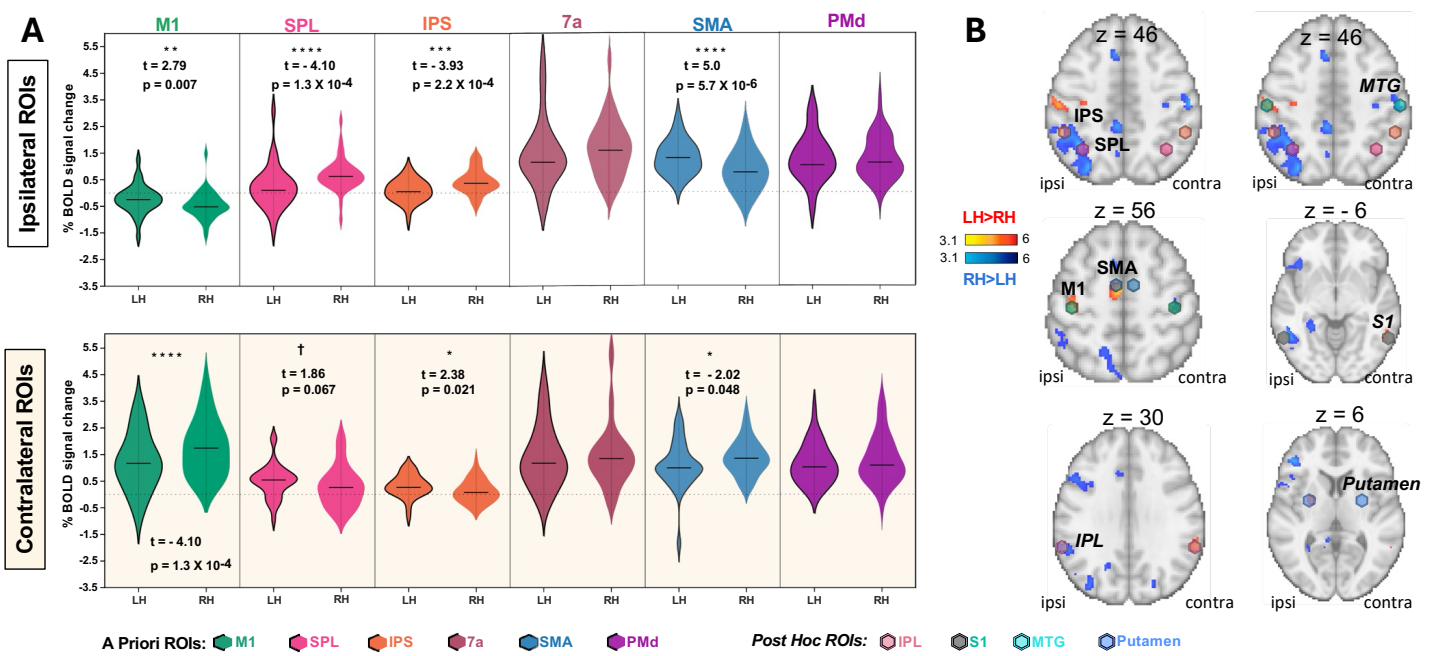

Figure 2: $Hand_{LH-RH}$ effects on BOLD magnitude. **A:** ROI analysis. The effect of $hand_{LH-RH}$ in M1/SMA is ipsilateral +, contralateral –; whereas in SPL/IPS, the effect is ipsilateral –, contralateral +. Statistics from GLME. **B**: Whole-brain analysis. 7 significant clusters were found, of which 4 were unique and used as seeds for 8 bilateral post hoc ROIs (italicized; see Table 5).

Exploratory whole-brain analysis reveals additional LH-specific parieto-temporal contributions

To explore effects of drawing hand on BOLD magnitude beyond our 12 apROIs, we performed an exploratory whole-brain group-level analysis of $hand_{LH-RH}$ (i.e. the contrast LH > RH). These whole-brain results (**Figure 2b**) included 7 clusters as listed in **Table 4**. The strongest two clusters overlapped our apROIs in M1-ipsi and SMA-ipsi. We found additional clusters in the inferior parietal lobule (IPL)-contra (two redundant clusters: timecourse correlation r = 0.812, p < 0.001), primary somatosensory cortex (S1-ipsi), putamen (Putamen-ipsi), and middle temporal gyrus (MTG-contra), as shown in **Table 4**. The unique

clusters served as seeds for bilateral post hoc ROIs (phROIs). Overall, this whole-brain exploration was consistent with, but expanded, our apROI analysis.

In addition, we assessed the effect of confounds on our $hand_{LH-RH}$ results via whole-brain group-level analyses of interaction effects. Only one confound factor, sexF, was strong enough for inclusion in any of our apROI analyses (see **Supplementary Table 4**) and thus tested here. However, a whole-brain analysis of the of the $hand_{LH-RH}$ * sexF interaction revealed no significant clusters.

Cluster Index	Voxels	p	Z-MAX	Z-COG X (mm)	Z-COG Y (mm)	Z-COG Z (mm)	Anatomical region	Post hoc ROI?
7	421	<0.001	4.85	-30.2	-17.8	66.1	M1 (ipsi)	No[1]
6	204	0.001	5.36	-6.92	-9.57	59	SMA (ipsi)	No[1]
5	136	0.013	5.46	61.6	-43.3	30.5	IPL (contra)	Yes[2]
4	125	0.019	4.76	-54	-21.1	44.4	S1 (ipsi)	Yes
3	121	0.021	4.21	-26.7	-2.06	5.28	Putamen (ipsi)	Yes
2	99	0.047	4.35	55.7	-54.2	-6.95	MTG (contra)	Yes
1	98	0.049	3.8	53.7	-54.1	39.1	IPL (contra)	No[2]

Table 4: Significant clusters in whole-brain contrast LH>RH ($hand_{LH-RH}$). Significance determined at cluster-corrected, $p < 0.05$. [1]: Overlapped with the apROI in the same region. [2]: Clusters #2 and #5 were correlated, so only #2 was used. Abbreviations: M1 = primary motor cortex; SMA = supplementary motor area; S1 = primary somatosensory cortex; IPL = inferior parietal lobule; MTG = middle temporal gyrus.

Functional Connectivity: LH drawing depends on bilateral parieto-motor interactions

We evaluated hand-specific modulation of FC between our apROIs via a gPPI analysis, which revealed positive modulation for $hand_{LH-RH}$ (i.e. LH > RH) in 5 connections between 6/12 ROIs, and no connections with negative modulation for $hand_{LH-RH}$ (RH > LH), as listed in **Table 5**. The positive $hand_{LH-RH}$ modulation included increased FC between M1-contra and both M1-ipsi and IPS-contra; between IPS-contra and SPL-contra; and between M1-ipsi and both SMA-contra and PMd-ipsi.

To contextualize this hand-dependent modulation, we examined traditional FC (not gPPI modulation) between ROIs, separately for each drawing condition relative to rest (LH > Rest; RH > Rest). All five connections identified by gPPI had FC > 0 in both conditions, with numerically stronger FC during LH (t-scores 7.31–12.64, $p < .001$, FDR/FWE = 0) than RH (t-scores 2.63–7.47, $p \leq .015$, FDR/FWE ≤ .00024). This indicates that the positive gPPI modulation for $hand_{LH-RH}$ reflects a strengthening of pre-existing positive connectivity.

ROI 1	ROI 2	T-score	p-value
PMd-ipsi	M1-ipsi	4.37	0.0160
M1-contra	M1-ipsi	4	0.0230
IPS-contra	SPL-contra	3.8	0.0272
M1-contra	IPS-contra	3.5	0.0453
SMA-contra	M1-ipsi	3.41	0.0470

Table 5: Connections between apROIs with significant $hand_{LH-RH}$ modulation of functional connectivity, assessed via gPPI. *P*-values corrected for false discovery rate.

Post-hoc power assessment indicates sufficient sensitivity for the observed magnitude effects

Because this study's sample size was chosen to detect effects in SPL-ipsi, we evaluated its sensitivity across ROIs via a simulation-based sensitivity (post hoc) power assessment in all other ROIs (apROI and phROI) with significant $hand_{LH-RH}$ effects. The minimum sample size required to reach 80% power was ≤ 30 in M1-ipsi, M1-contra, SPL-ipsi, IPL-ipsi, IPL-contra, S1-contra, and MTG-contra; however, larger samples sizes were required in IPS-contra (n=50), SMA-contra (n=65), and Putamen-contra (n=140). Therefore, based on our sample size of N=33, this study was sufficiently sensitive to detect $hand_{LH-RH}$ effects in most ROIs.

Separately, to quantify data quality, we evaluated the SNR of the task effect on BOLD magnitude. This study achieved SNR 0.487 ± 0.07, approaching the 0.5 upper end of task fMRI effects (Masharipov et al., 2024a).

Post hoc areas: during LH drawing, magnitude and connectivity increase in contralateral hemisphere, decrease in parieto-temporal areas and left inferior parietal lobule

Based on our post-hoc power assessment, our study was sufficiently sensitive to detect $hand_{LH-RH}$ effects not only in many apROIs, but also in many phROIs.

We evaluated BOLD magnitude in our phROIs via our GLME approach. Statistical results in half of the phROIs would be invalid due to double-dipping, so full results are in **Supplementary Table 5**. Overall, BOLD magnitude in the post-hoc ROIs followed the motor-like pattern (LH>RH) in S1 and Putamen, and the parietal-like pattern (RH>LH) in IPL and MTG.

To evaluate FC modulation involving our post-hoc ROIs, we repeated the gPPI analysis with all 20 ROIs (12 a priori, 8 post hoc). Full results are in **Supplementary Figure**, but to constrain our interpretation of post-hoc analyses, we did not interpret connections that would convert a negative a priori result to a positive one (i.e., if an apROI lacked significant FC modulation in our previous gPPI analysis, we do not interpret its connections here). Following this constraint, we found $hand_{LH-RH}$ FC modulation in 7 new connections involving 4/8 phROIs: positive $hand_{LH-RH}$ modulation between MTG-contra and each of PMd-ipsi ($t = 3.28$, $p = 0.043$), M1-contra ($t = 3.91$, $p = 0.019$), and S1-contra ($t = 4.69$, $p = 0.006$); positive $hand_{LH-RH}$ modulation between IPL-contra and both M1-contra ($t = 3.25$, $p = 0.045$) and S1-contra ($t = 4.39$m $p = 0.006$); and negative $hand_{LH-RH}$ modulation between M1-contra and IPL-ipsi ($t = -3.71$, $p = 0.025$).

Maginitude-Connectivity Integration: during LH drawing, right M1 decreases magnitude but increases connectivity with left motor-premotor and right parietal-occipital areas.

To integrate our fMRI analyses of our apROIs, we visualized our BOLD magnitude and FC modulation effects together in **Figure 3a**. Together, these results show that the $hand_{LH-RH}$ effect involved the corticospinal output area M1-contra reducing magnitude but increasing connectivity. Specifically, for $hand_{LH-RH}$ drawing, M1-contra had stronger interhemispheric FC with M1-ipsi, which had higher magnitude and stronger FC with PMd-ipsi and SMA-contra. At the same time, M1-contra also had stronger intrahemisphereric FC with contralateral parietal regions (IPS, SPL) that may potentially have higher magnitude.

We expanded this integrative visualization to encompass our phROIs in **Figure 3b**, which fits but extends the patterns found in apROIs. The phROIs expanded the group of "contralateral intrahemispheric" areas to include IPL and MTG, which had higher magnitude during LH drawing. S1-contra followed the same pattern as M1-contra: lower magnitude, but increased FC with higher-magnitude areas (here, IPS-contra and MTG-contra). The post-hoc ROIs added one a third $hand_{LH-RH}$ effect: IPL-ipsi had lower magnitude and weaker interhemispheric FC with M1-contra.

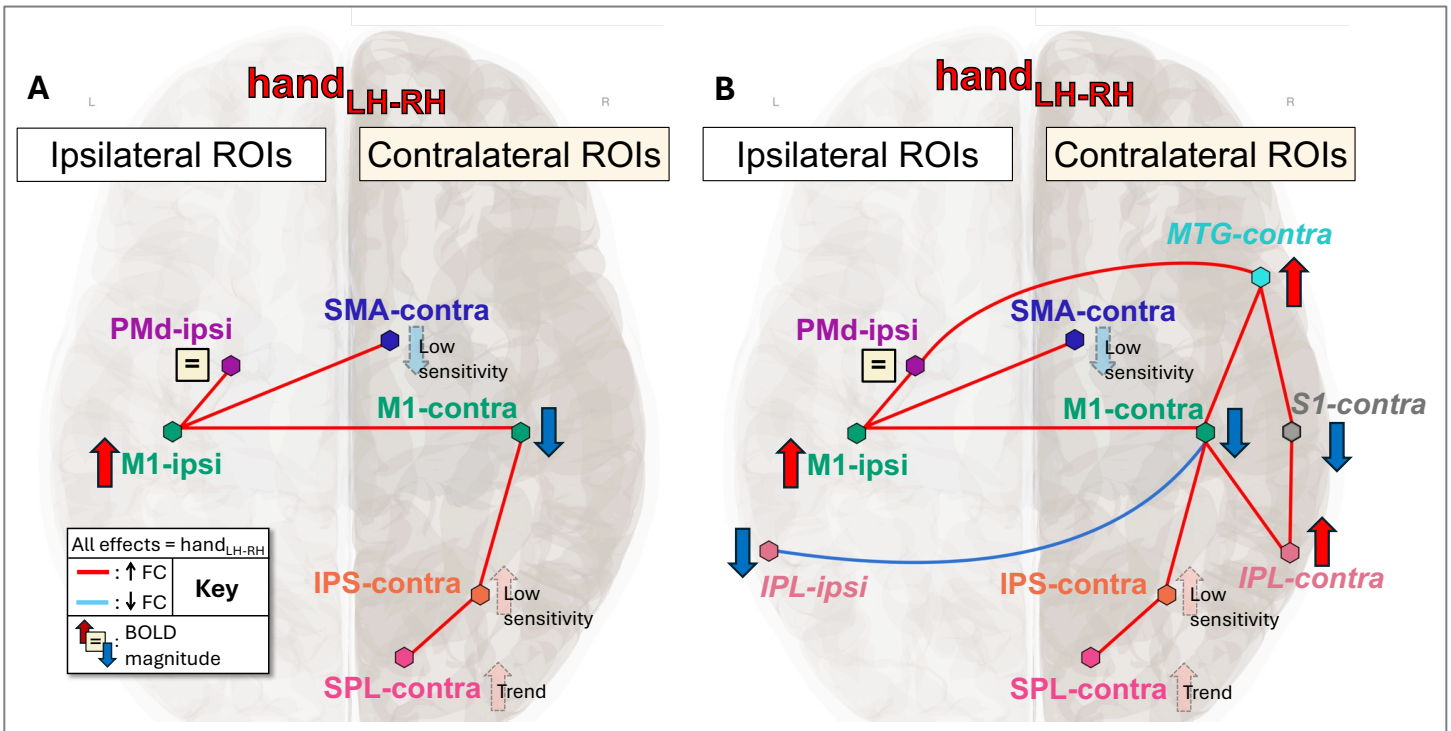

Figure 3: Integrated visualization of BOLD magnitude and functional connectivity (FC) modulation for $hand_{LH-RH}$. ROIs are shown if any of their connections had significant gPPI modulation (lines); if shown, BOLD magnitude differences (arrows) are overlaid. For visual clarity, ROI locations are illustrative. *P*-values = FDR-corrected. "Low sensitivity" based on post-hoc power assessment. **A**: Analysis of a priori ROIs. **B**: Analysis of all ROIs: 12 a priori + 8 post hoc (italicized).

Overall, by combining BOLD magnitude and FC modulation, our results indicate that, during LH precision drawing, motor output (i.e. M1-contra) is primarily supported by ipsilateral left motor-premotor and contralateral right parieto-temporal areas.

Patients with peripheral nerve injury show the same hand-specific effects as healthy adults

To address our hypothesis that patients with chronic PNI would use the same neural mechanisms as healthy adults for LH drawing, we first evaluated whether Group (patient vs. control) contributed to any GLME of BOLD magnitude. Group was not strong enough to be included in any GLME model (**Supplementary Table 4**), and its univariate p-value never exceeded 0.200 in any ROI (**Supplementary Table 3**). To confirm this negative result, we evaluated the univariate effect size of Group in each ROI, and found that its 95% confidence interval included zero in all ROIs.

Patient group also had no effect on whole-brain BOLD magnitude: no significant clusters for Patient > Control, Control > Patient, nor for the interactions Group*$Hand_{LH-RH}$ or Group*SexF. Therefore, we found no evidence that BOLD magnitude $hand_{LH-RH}$ effects differed between patients and controls.

We found no effect of patient group on functional connectivity.

DISCUSSION

Our study used a visually-guided precision drawing task to characterize neural activity and functional connectivity associated with left hand (LH) drawing, in right-handed individuals with and without unilateral RH peripheral nerve injury (PNI). We identified two mechanisms that supported LH precision drawing, and one specific to RH precision drawing, as shown in **Figure 4**. Overall, control of the non-preferred LH was achieved by a combination of two factors: motor output (right M1) was supported by

adapting a dominant (left) hemisphere motor-premotor circuit via enhanced interhemispheric integration, and increasing intrahemispheric engagement of secondary motor areas in the contralateral hemisphere. The performance differences between the LH and RH may be explained by right M1's indirect connections to the left motor-premotor circuit, and its incomplete access to a parietal circuit for tool use. These neural mechanisms did not differ between healthy adults and patients with chronic RH PNI.

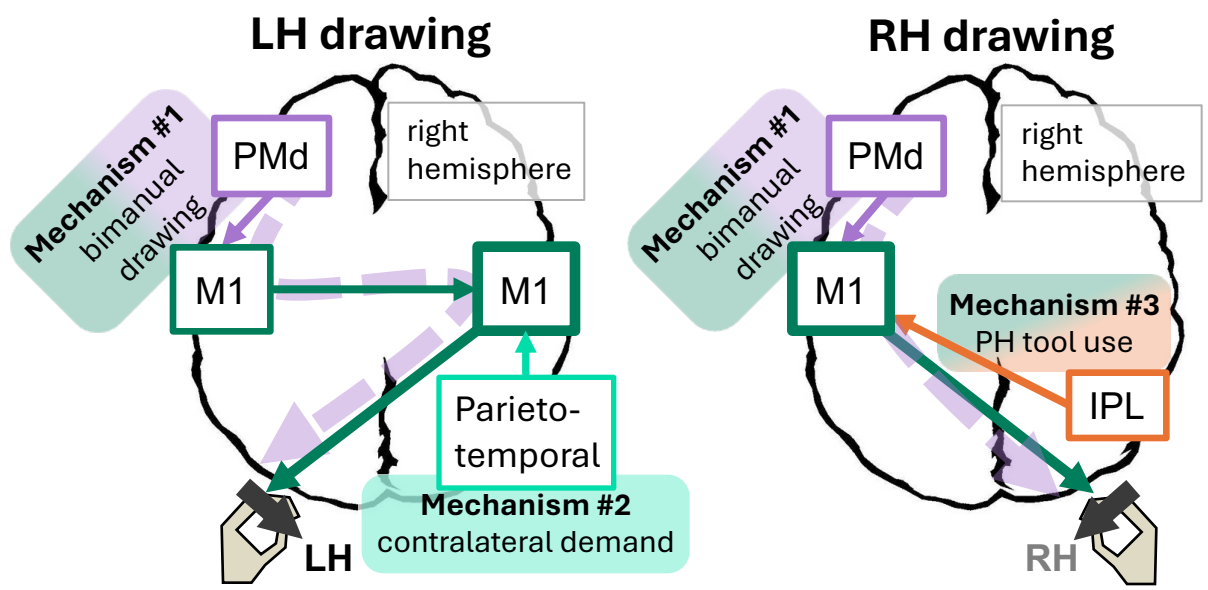

Figure 4: Model of neural mechanisms with differential involvement in left hand (LH) vs. right hand (RH) precision drawing. **Mechanism #1** is a left M1-PMd circuit for bimanual drawing, with access to contralateral M1 via hand-specific paths (dashed lines): an indirect interhemispheric path during LH drawing, and a direct intrahemispheric path during RH drawing. **Mechanism #2** is an intrahemispheric parieto-temporal network for LH drawing, potentially representing increased engagement of contralateral secondary motor systems to support high-demand action. **Mechanism #3** is an interhemispheric M1-IPL circuit for RH drawing, potentially reflecting a unique lateralization for tool use and praxis with the preferred hand (PH) in right-handed adults.

A left-hemisphere motor-premotor circuit supports bimanual precision drawing

We found a left-lateralized M1-PMd circuit that functions as a shared neural mechanism for bimanual precision drawing in right-handed adults. We consider this our primary finding because it is the only mechanism entirely composed of apROIs. This circuit may involve M1's role in ipsilateral movement under complex or high-demand conditions (Barany et al., 2020; Buetefisch et al., 2014; Kim et al., 1993; Verstynen et al., 2005) and left PMd's role in for temporal aspects of bilateral movement (Kornysheva & Diedrichsen, 2014; Schluter et al., 1998) and their associated task-specific demands (Yang et al., 2024). During RH drawing, this circuit includes the source of descending corticospinal control in contralateral left M1. During LH drawing, this circuit does not include contralateral (right) M1, so it contributes to descending control via interhemispheric connectivity. In other words, the left-lateralized M1-PMd system retains its role across hands by adaptively recruiting – or being recruited by – contralateral motor regions via interhemispheric M1-M1 connections (**Figure 4**, Mechanism #1).

This left-lateralized M1-PMd circuit provides anatomical specificity to existing models of hand dominance, which posit that RH advantages (in right-handed individuals) arise from a left hemisphere specialization for precise trajectories, and LH disadvantages arise from interhemispheric delays(Kitchen et al., 2025; Liepmann, 1905; B. A. Shabbott & R. L. Sainburg, 2008) is consistent with previous findings that FC in a M1-PMd-somatosensory network supports precision manual tasks with the RH (Yang et al., 2024). Here we show that this left-lateralized mechanism connects to cortical outputs via a hand-specific path: direct intrahemispheric during RH drawing, and indirect interhemispheric during LH drawing.

Our effector-independent role for left PMd diverges from the findings of Potgieser et al. (2015), who reported bilateral PMd activation during a visually guided figure-copying task. This difference may depend on task characteristics: unlike Potgieser et al. (2015), our task imposed constrains on spatial precision, which affects lateralization across parietal and premotor cortices (Haaland et al., 2004).

A right parieto-temporal network supports the execution of demanding tasks with the left hand.
We identified a parieto-temporal network (SPL, IPS, IPL, MTG) that became more engaged with right M1 for $hand_{LH-RH}$. This network had greater intrahemispheric (right hemisphere) connectivity with right M1 alongside modest increases in activity (significant in IPL/MTG, trend in SPL, under-powered in IPS). Right posterior parietal areas are involved in various aspects of visuomotor control: goal-directed visuospatial attention (Corbetta et al., 2000; Wang et al., 2016), combining and maintaining representations of goal and movement (Averbeck et al., 2009; Wolpert et al., 1998), motor skill learning (Della-Maggiore et al., 2004), and action planning with the contralateral hand (Valyear & Frey, 2015); and the roles of right MTG include monitoring intersensory conflict (van Kemenade et al., 2019) and the visual evaluation of action quality (Jastorff et al., 2010). This network is unlikely to represent the right hemisphere's specializations for impedence components of movement (Kitchen et al., 2025), because such a specalization should show increased interhemispheric connectivity during RH drawing (when a right hemisphere mechanism supports left M1). Therefore, we propose that the right parieto-temporal network represents a broad contralateral-hemisphere sensorimotor control network that becomes more engaged during LH drawing due to the increased task demands of in drawing with the non-preferred hand (**Figure 4**, Mechanism #2).

An interhemispheric parietal-motor circuit supports tool use and praxis with the right hand.
We found differential $hand_{LH-RH}$ disengagement of ipsilateral IPL: it had lower activity, and its interhemispheric IPL-M1 connection was the only connection with negative modulation for $hand_{LH-RH}$. This unique disengagement suggests a mechanism that supports drawing with the preferred RH but (unlike Mechanism #1) is not effectively adapted to support LH drawing. IPL is involved in sensorimotor integration for praxis and tool use, though it remains unclear whether those functions are lateralized to left IPL (Buxbaum et al., 2007; Rosenzopf et al., 2022; Wheaton et al., 2009) or right IPL (Ras et al., 2022; Singh-Curry & Husain, 2009). This is consistent with our use of a task involving a tool with high sensorimotor control demands (drawing with a stylus, in an unfamiliar position, viewed with a mirror). Therefore, we propose that the interhemispheric IPL-M1 circuit represents a mechanism for tool use with the preferred hand (**Figure 4**, Mechanism #3).

Patients with PNI control their LH via the same mechanisms as healthy adults
Participants with chronic RH PNI recruited the same three mechanisms as healthy controls, implying that all three mechanisms remain intact and accessible after chronic unilateral PNI. Its engagement during LH drawing in patients carries promising clinical implications, as it provides a target for neuromodulatory or behavioral interventions aimed at improving NPH function. Multiple rehabilitation approaches have demonstrated efficacy in enhancing NPH performance, including bimanual training (Stinear & Byblow,

2004), mirror therapy (Dohle et al., 2009; Nojima et al., 2012), action observation (Ertelt et al., 2007), motor imagery (Sharma et al., 2006), and bihemispheric stimulation strategies such as dual tDCS or rTMS (Lindenberg et al., 2010; Waters-Metenier et al., 2014). These approaches converge on the principle that bilateral cortical recruitment, particularly via the dominant hemisphere, can facilitate motor recovery or compensation after unilateral impairment.

In addition, this work helps establish a normative template of bilateral cortical control for precision movement in the healthy brain. Such a benchmark is critical for rehabilitation of asymmetric neurological conditions such as stroke, wherein some patients must rely on their NPH due to chronic PH impairment. For example, researchers and clinicians can now determine whether a patient is using their NPH with a typical brain mechanism (i.e. the left M1-PMd circuit) versus an atypical brain mechanism, or whether reduced interhemispheric connectivity might impede the typical mechanism. This will allow researchers to characterize atypical mechanisms, and may allow clinicians to predict which patients can learn to effectively use their NPH. Overall, our study provides the essential groundwork to identify atypical and pathological neural mechanisms, and ultimately to design individualized, mechanism-driven rehabilitation protocols that improve outcomes and restore function across a range of unilateral motor impairments.

Ipsilateral SPL may be learning-dependent

Our results did not support our initial hypothesis that a locus in ipsilateral SPL would play a greater role during LH than RH drawing. We based this hypothesis on previous findings that interhemispheric FC involving ipsilateral left SPL could predict future LH skill learning (Philip et al., 2021). However, the current study did not involve learning: participants completed only 5.5 minutes of familiarization with each hand, followed by 16.5 minutes with each hand during fMRI, far below the amount of time required to learn a NPH precision drawing task (4.6 ± 2.3 sessions of 20 minutes each; Philip & Frey, 2016). Therefore, our our SPL locus may be capture a mechanism specific to learning of NPH skill (Philip et al., 2021).

Limitations

The sample size for this study was calculated from an *a priori* power analysis of preliminary data to identify an effect of hand (LH vs. RH) in ipsilateral SPL. However, our primary hypothesis was not supported, and thus we drew conclusions from secondary ROIs. Moreover, our a *priori* design meant that gPPI was a secondary analysis. Simulation studies suggest $n \geq 50$ to detect gPPI effects in a block design study of SNR ~0.5 (Masharipov et al., 2024a). For gPPI and covariate analyses (e.g. performance), further studies with larger sample sizes are necessary.

Our current analysis confounds hand and task demands (i.e. LH movements are more difficult). Due to this limitation we present our interpretation of Mechanism #2 (contralateral task demand) as a hypothesis, which will be tested in future analyses that independently manipulate hand and task demands.

Our results describe neural mechanisms specific to the control of precision drawing (a PH-specialized task) in right-handed adults. Therefore, our findings provide no information about neural mechanisms of NPH specializations, nor about left-handed individuals.

Conclusion

This study identified three neural mechanisms that distinguish LH vs. RH drawing in right-handed adults. First, a lateralized M1-PMd circuit for bilateral control, which is engaged interhemispherically during LH drawing and intrahemispherically during RH drawing. Second, LH drawing increases engagement in a contralateral parietotemporal circuit, potentially due to the difficulty of LH drawing. Third, RH drawing

increases engagement of an interhemispheric parietal-motor circuit, potentially for tool use. In addition, individuals with chronic PNI to their right hand used the same neural mechanisms, indicating that cortical adaptation after injury may leverage pre-existing dominant-hemisphere and interhemispheric circuitry.

These findings provide a specific neuroanatomical basis for existing theories of handedness, including a potential neural mechanism for observed behavioral asymmetries in upper limb performance. The left M1–PMd circuit's role in bilateral control highlights it as a compelling target for neuromodulatory and rehabilitative interventions to enhance motor function after injury.

References

Abraham, A., Pedregosa, F., Eickenberg, M., Gervais, P., Mueller, A., Kossaifi, J., Gramfort, A., Thirion, B., & Varoquaux, G. (2014). Machine learning for neuroimaging with scikit-learn. *Frontiers in neuroinformatics*, *8*, 14.

Avants, B. B., Epstein, C. L., Grossman, M., & Gee, J. C. (2008). Symmetric diffeomorphic image registration with cross-correlation: evaluating automated labeling of elderly and neurodegenerative brain. *Medical image analysis*, *12*(1), 26-41.

Averbeck, B. B., Crowe, D. A., Chafee, M. V., & Georgopoulos, A. P. (2009). Differential contribution of superior parietal and dorsal-lateral prefrontal cortices in copying. *Cortex*, *45*(3), 432-441. https://doi.org/10.1016/j.cortex.2008.02.007

Barany, D. A., Revill, K. P., Caliban, A., Vernon, I., Shukla, A., Sathian, K., & Buetefisch, C. M. (2020). Primary motor cortical activity during unimanual movements with increasing demand on precision. *Journal of Neurophysiology*, *124*(3), 728-739.

Behzadi, Y., Restom, K., Liau, J., & Liu, T. T. (2007). A component based noise correction method (CompCor) for BOLD and perfusion based fMRI. *NeuroImage*, *37*(1), 90-101. https://doi.org/10.1016/j.neuroimage.2007.04.042

Blank, R., Miller, V., & Von Voss, H. (2000). Human motor development and hand laterality: a kinematic analysis of drawing movements. *Neuroscience Letters*, *295*(3), 89-92.

Buetefisch, C. M., Revill, K. P., Shuster, L., Hines, B., & Parsons, M. (2014). Motor demand-dependent activation of ipsilateral motor cortex. *Journal of Neurophysiology*, *112*(4), 999-1009. https://doi.org/10.1152/jn.00110.2014

Buxbaum, L. J., Kyle, K., Grossman, M., & Coslett, B. (2007). Left inferior parietal representations for skilled hand-object interactions: evidence from stroke and corticobasal degeneration. *Cortex*, *43*(3), 411-423.

Caviness Jr, V. S., Meyer, J., Makris, N., & Kennedy, D. N. (1996). MRI-based topographic parcellation of human neocortex: an anatomically specified method with estimate of reliability. *Journal of Cognitive Neuroscience*, *8*(6), 566-587.

Corbetta, M., Kincade, J. M., Ollinger, J. M., McAvoy, M. P., & Shulman, G. L. (2000). Voluntary orienting is dissociated from target detection in human posterior parietal cortex. *Nature neuroscience*, *3*(3), 292-297.

Dale, A. M., Fischl, B., & Sereno, M. I. (1999). Cortical surface-based analysis: I. Segmentation and surface reconstruction. *NeuroImage*, *9*(2), 179-194.

Della-Maggiore, V., Malfait, N., Ostry, D. J., & Paus, T. (2004). Stimulation of the posterior parietal cortex interferes with arm trajectory adjustments during the learning of new dynamics. *The Journal of Neuroscience: the Official Journal of the Society for Neuroscience*, *24*(44), 9971-9976. https://doi.org/10.1523/JNEUROSCI.2833-04.2004

Desikan, R. S., Segonne, F., Fischl, B., Quinn, B. T., Dickerson, B. C., Blacker, D., Buckner, R. L., Dale, A. M., Maguire, R. P., Hyman, B. T., Albert, M. S., & Killiany, R. J. (2006). An automated labeling system for subdividing the human cerebral cortex on MRI scans into gyral based regions of interest. *NeuroImage*, *31*(3), 968-980. https://doi.org/10.1016/j.neuroimage.2006.01.021

Dexheimer, B., Sainburg, R. L., Sharp, S., & Philip, B. A. (2024). Roles of Handedness and Hemispheric Lateralization: Implications for Rehabilitation of the Central and Peripheral Nervous Systems: A Rapid Review. *American Journal of Occupational Therapy*, *78*(2). https://doi.org/10.5014/ajot.2024.050398

Dohle, C., Püllen, J., Nakaten, A., Küst, J., Rietz, C., & Karbe, H. (2009). Mirror Therapy Promotes Recovery From Severe Hemiparesis: A Randomized Controlled Trial. *Neurorehabilitation and Neural Repair*, *23*(3), 209-217. https://doi.org/10.1177/1545968308324786

Eickhoff, S., Heim, S., Zilles, K., & Amunts, K. (2006). Testing anatomically specified hypotheses in functional imaging using cytoarchitectonic maps. *NeuroImage*, *32*(2), 570-582. https://doi.org/10.1016/j.neuroimage.2006.04.204

Eickhoff, S. B., Paus, T., Caspers, S., Grosbras, M.-H., Evans, A. C., Zilles, K., & Amunts, K. (2007). Assignment of functional activations to probabilistic cytoarchitectonic areas revisited. [Review]. *NeuroImage*, *36*(3), 511-521. https://doi.org/10.1016/j.neuroimage.2007.03.060

Ertelt, D., Small, S., Solodkin, A., Dettmers, C., McNamara, A., Binkofski, F., & Buccino, G. (2007). Action observation has a positive impact on rehabilitation of motor deficits after stroke. *NeuroImage*, *36*, T164-T173. https://doi.org/https://doi.org/10.1016/j.neuroimage.2007.03.043

Esteban, O., Markiewicz, C. J., Blair, R. W., Moodie, C. A., Isik, A. I., Erramuzpe, A., Kent, J. D., Goncalves, M., DuPre, E., & Snyder, M. (2019). fMRIPrep: a robust preprocessing pipeline for functional MRI. *Nature methods*, *16*(1), 111-116.

Fonov, V. S., Evans, A. C., McKinstry, R. C., Almli, C. R., & Collins, D. (2009). Unbiased nonlinear average age-appropriate brain templates from birth to adulthood. *NeuroImage*, *47*, S102.

Freud, E., Macdonald, S. N., Chen, J., Quinlan, D. J., Goodale, M. A., & Culham, J. C. (2018). Getting a grip on reality: Grasping movements directed to real objects and images rely on dissociable neural representations. *Cortex*, *98*, 34-48. https://doi.org/10.1016/j.cortex.2017.02.020

Gorgolewski, K., Burns, C. D., Madison, C., Clark, D., Halchenko, Y. O., Waskom, M. L., & Ghosh, S. S. (2011). Nipype: a flexible, lightweight and extensible neuroimaging data processing framework in python. *Frontiers in neuroinformatics*, *5*, 13.

Green, P., MacLeod, C. J., & Nakagawa, S. (2016). SIMR: an R package for power analysis of generalized linear mixed models by simulation. *Methods in Ecology and Evolution*, *7*(4), 493-498. https://doi.org/10.1111/2041-210x.12504

Greve, D. N., & Fischl, B. (2009). Accurate and robust brain image alignment using boundary-based registration. [Evaluation Study]. *NeuroImage*, *48*(1), 63-72. https://doi.org/10.1016/j.neuroimage.2009.06.060

Haaland, K. Y., Elsinger, C. L., Mayer, A. R., Durgerian, S., & Rao, S. M. (2004). Motor sequence complexity and performing hand produce differential patterns of hemispheric lateralization. *Cognitive Neuroscience, Journal of*, *16*(4), 621-636. http://ieeexplore.ieee.org/xpls/abs_all.jsp?arnumber=6789895

Hayashi, M. J., Saito, D. N., Aramaki, Y., Asai, T., Fujibayashi, Y., & Sadato, N. (2008). Hemispheric asymmetry of frequency-dependent suppression in the ipsilateral primary motor cortex during finger movement: a functional magnetic resonance imaging study. *Cereb Cortex*, *18*(12), 2932-2940. https://doi.org/10.1093/cercor/bhn053

Jastorff, J., Clavagnier, S., Gergely, G., & Orban, G. A. (2010). Neural Mechanisms of Understanding Rational Actions: Middle Temporal Gyrus Activation by Contextual Violation. *Cerebral Cortex*, *21*(2), 318-329. https://doi.org/10.1093/cercor/bhq098

Jenkinson, M., Bannister, P., Brady, M., & Smith, S. (2002). Improved optimization for the robust and accurate linear registration and motion correction of brain images. *NeuroImage*, *17*(2), 825-841.

Jenkinson, M., Beckmann, C. F., Behrens, T. E. J., Woolrich, M. W., & Smith, S. M. (2012). FSL. *NeuroImage*, *62*(2), 782-790. https://doi.org/https://doi.org/10.1016/j.neuroimage.2011.09.015

Karimpoor, M., Churchill, N. W., Tam, F., Fischer, C. E., Schweizer, T. A., & Graham, S. J. (2018). Functional MRI of Handwriting Tasks: A Study of Healthy Young Adults Interacting with a Novel Touch-Sensitive Tablet. *Front Hum Neurosci*, *12*, 30. https://doi.org/10.3389/fnhum.2018.00030

Karimpoor, M., Tam, F., Strother, S. C., Fischer, C. E., Schweizer, T. A., & Graham, S. J. (2015). A computerized tablet with visual feedback of hand position for functional magnetic resonance imaging. *Frontiers in Human Neuroscience*, *9*, 150.

Kim, S. G., Ashe, J., Hendrich, K., Ellermann, J. M., Merkle, H., Uğurbil, K., & Georgopoulos, A. P. (1993). Functional magnetic resonance imaging of motor cortex: hemispheric asymmetry and handedness. *Science*, *261*(5121), 615-617. https://doi.org/10.1126/science.8342027

Kim, T., Gassass, S., Carter, A. R., Dobbins, I. G., Liu, L., McAvoy, M., Sun, Z., Wang, Y., & Philip, B. A. (2023). *Ipsilateral parietal cortex supports precision movement with the non-dominant hand* Progress in Clinical Motor Control II, Chicago, IL.

Kitchen, N. M., Dexheimer, B., Yuk, J., Maenza, C., Ruelos, P. R., Kim, T., & Sainburg, R. L. (2025). The complementary dominance hypothesis: a model for remediating the 'good' hand in stroke survivors. *Journal of Physiology*, *603*(3), 663-683. https://doi.org/10.1113/JP285561

Klein, A., Ghosh, S. S., Bao, F. S., Giard, J., Häme, Y., Stavsky, E., Lee, N., Rossa, B., Reuter, M., & Chaibub Neto, E. (2017). Mindboggling morphometry of human brains. *PLoS Computational Biology*, *13*(2), e1005350.

Kornysheva, K., & Diedrichsen, J. (2014). Human premotor areas parse sequences into their spatial and temporal features. *Elife*, *3*, e03043. https://doi.org/10.7554/eLife.03043

Kriegeskorte, N., Simmons, W. K., Bellgowan, P. S., & Baker, C. I. (2009). Circular analysis in systems neuroscience: the dangers of double dipping. *Nat Neurosci*, *12*(5), 535-540. https://doi.org/10.1038/nn.2303

Liepmann, H. M. O. (1905). Die linke Hemisphäre und das Handeln. Münchener Medizinische Wochenschrift. (49), 2322–2326, 2375–2378.

Liesefeld, H. R., & Janczyk, M. (2023). Same same but different: Subtle but consequential differences between two measures to linearly integrate speed and accuracy (LISAS vs. BIS). *Behav Res Methods*, *55*(3), 1175-1192. https://doi.org/10.3758/s13428-022-01843-2

Lindenberg, R., Renga, V., Zhu, L. L., Nair, D., & Schlaug, G. (2010). Bihemispheric brain stimulation facilitates motor recovery in chronic stroke patients. *Neurology*, *75*(24), 2176-2184. https://doi.org/10.1212/wnl.0b013e318202013a

Mani, S., Mutha, P. K., Przybyla, A., Haaland, K. Y., Good, D. C., & Sainburg, R. L. (2013). Contralesional motor deficits after unilateral stroke reflect hemisphere-specific control mechanisms. *Brain*, *136*(Pt 4), 1288-1303. https://doi.org/10.1093/brain/aws283

Masharipov, R., Knyazeva, I., Korotkov, A., Cherednichenko, D., & Kireev, M. (2024a). Comparison of whole-brain task-modulated functional connectivity methods for fMRI task connectomics. *Commun Biol*, *7*. https://doi.org/10.1101/2024.01.22.576622

Masharipov, R., Knyazeva, I., Korotkov, A., Cherednichenko, D., & Kireev, M. (2024b). Comparison of whole-brain task-modulated functional connectivity methods for fMRI task connectomics. *Communications Biology*, *7*(1). https://doi.org/10.1038/s42003-024-07088-3

McLaren, D. G., Ries, M. L., Xu, G., & Johnson, S. C. (2012). A generalized form of context-dependent psychophysiological interactions (gPPI): a comparison to standard approaches. *NeuroImage*, *61*(4), 1277-1286. https://doi.org/10.1016/j.neuroimage.2012.03.068

Mumford, J. A. (2012). A power calculation guide for fMRI studies. *Soc Cogn Affect Neurosci*, *7*(6), 738-742. https://doi.org/10.1093/scan/nss059

Mumford, J. A. (2017). *FEAT registration workaround*. Retrieved June 1 from https://mumfordbrainstats.tumblr.com/post/166054797696/feat-registration-workaround

Nieto-Castanon, A. (2020). *Handbook of functional connectivity Magnetic Resonance Imaging methods in CONN*. https://doi.org/10.56441/hilbertpress.2207.6598

Nojima, I., Mima, T., Koganemaru, S., Thabit, M. N., Fukuyama, H., & Kawamata, T. (2012). Human Motor Plasticity Induced by Mirror Visual Feedback. *The Journal of Neuroscience*, *32*(4), 1293-1300. https://doi.org/10.1523/jneurosci.5364-11.2012

Patriat, R., Reynolds, R. C., & Birn, R. M. (2017). An improved model of motion-related signal changes in fMRI. *NeuroImage*, *144*, 74-82.

Philip, B. A., & Frey, S. H. (2014). Compensatory Changes Accompanying Chronic Forced Use of the Nondominant Hand by Unilateral Amputees. *The Journal of Neuroscience: the Official Journal of the Society for Neuroscience*, *34*(10), 3622-3631. https://doi.org/10.1523/JNEUROSCI.3770-13.2014

Philip, B. A., & Frey, S. H. (2016). Increased functional connectivity between cortical hand areas and praxis network associated with training-related improvements in non-dominant hand precision drawing. *Neuropsychologia*, *87*, 157-168. https://doi.org/10.1016/j.neuropsychologia.2016.05.016

Philip, B. A., Li, F., Hawkins-Chernof, E., Swamidass, V., & Zwir, I. (2023). Motor Assessment With the STEGA iPad App to Measure Handwriting in Children. *American Journal of Occupational Therapy*, *77*(3).

Philip, B. A., McAvoy, M. P., & Frey, S. H. (2021). Interhemispheric Parietal-Frontal Connectivity Predicts the Ability to Acquire a Nondominant Hand Skill. *Brain Connectivity*, *11*(4). https://doi.org/10.1089/brain.2020.0916

Pool, E. M., Rehme, A. K., Fink, G. R., Eickhoff, S. B., & Grefkes, C. (2014). Handedness and effective connectivity of the motor system. *NeuroImage*, *99*, 451-460. https://doi.org/10.1016/j.neuroimage.2014.05.048

Potgieser, A. R., van der Hoorn, A., & de Jong, B. M. (2015). Cerebral activations related to writing and drawing with each hand. *PLoS ONE*, *10*(5), e0126723. https://doi.org/10.1371/journal.pone.0126723

Ras, M., Wyrwa, M., Stachowiak, J., Buchwald, M., Nowik, A. M., & Kroliczak, G. (2022). Complex tools and motor-to-mechanical transformations. *Sci Rep*, *12*(1), 8041. https://doi.org/10.1038/s41598-022-12142-3

Rosenzopf, H., Wiesen, D., Basilakos, A., Yourganov, G., Bonilha, L., Rorden, C., Fridriksson, J., Karnath, H. O., & Sperber, C. (2022). Mapping the human praxis network: an investigation of white matter disconnection in limb apraxia of gesture production. *Brain Commun*, *4*(1), fcac004. https://doi.org/10.1093/braincomms/fcac004

Sainburg, R. L. (2002). Evidence for a dynamic-dominance hypothesis of handedness. *Experimental brain research Experimentelle Hirnforschung Expérimentation cérébrale*, *142*(2), 241-258. https://doi.org/10.1007/s00221-001-0913-8

Satterthwaite, T. D., Elliott, M. A., Gerraty, R. T., Ruparel, K., Loughead, J., Calkins, M. E., Eickhoff, S. B., Hakonarson, H., Gur, R. C., & Gur, R. E. (2013). An improved framework for confound regression and filtering for control of motion artifact in the preprocessing of resting-state functional connectivity data. *NeuroImage*, *64*, 240-256.

Schaefer, S. Y., Haaland, K. Y., & Sainburg, R. L. (2009). Hemispheric specialization and functional impact of ipsilesional deficits in movement coordination and accuracy. *Neuropsychologia*, *47*(13), 2953-2966. https://doi.org/10.1016/j.neuropsychologia.2009.06.025

Schaefer, S. Y., Mutha, P. K., Haaland, K. Y., & Sainburg, R. L. (2012). Hemispheric specialization for movement control produces dissociable differences in online corrections after stroke. *Cereb Cortex*, *22*(6), 1407-1419. https://doi.org/10.1093/cercor/bhr237

Schluter, N. D., Rushworth, M. F., Passingham, R. E., & Mills, K. R. (1998). Temporary interference in human lateral premotor cortex suggests dominance for the selection of movements. A study using transcranial magnetic stimulation. *Brain*, *121 (Pt 5)*, 785-799. https://doi.org/10.1093/brain/121.5.785

Seidman, L. J., Faraone, S. V., Goldstein, J. M., Goodman, J. M., Kremen, W. S., Toomey, R., Tourville, J., Kennedy, D., Makris, N., & Caviness, V. S. (1999). Thalamic and amygdala–hippocampal volume reductions in first-degree relatives of patients with schizophrenia: an MRI-based morphometric analysis. *Biological Psychiatry*, *46*(7), 941-954.

Shabbott, B. A., & Sainburg, R. L. (2008). Differentiating between two models of motor lateralization. *J Neurophysiol*, *100*(2), 565-575. https://doi.org/10.1152/jn.90349.2008

Shabbott, B. A., & Sainburg, R. L. (2008). Differentiating between two models of motor lateralization. *Journal of Neurophysiology*, *100*(2), 565-575. https://doi.org/10.1152/jn.90349.2008

Sharma, N., Pomeroy, V. M., & Baron, J.-C. (2006). Motor Imagery. *Stroke*, *37*(7), 1941-1952. https://doi.org/10.1161/01.str.0000226902.43357.fc

Singh-Curry, V., & Husain, M. (2009). The functional role of the inferior parietal lobe in the dorsal and ventral stream dichotomy. *Neuropsychologia*, *47*(6), 1434-1448. https://doi.org/10.1016/j.neuropsychologia.2008.11.033

Smith, S. M., Jenkinson, M., Woolrich, M. W., Beckmann, C. F., Behrens, T. E. J., Johansen-Berg, H., Bannister, P. R., De Luca, M., Drobnjak, I., Flitney, D. E., Niazy, R. K., Saunders, J., Vickers, J., Zhang, Y., De Stefano, N., Brady, J. M., & Matthews, P. M. (2004). Advances in functional and structural MR image analysis and implementation as FSL. [Review]. *NeuroImage*, *23 Suppl 1*, S208-219. https://doi.org/10.1016/j.neuroimage.2004.07.051

Stinear, C. M., & Byblow, W. D. (2004). Impaired modulation of intracortical inhibition in focal hand dystonia. *Cereb Cortex*, *14*(5), 555-561. https://doi.org/10.1093/cercor/bhh017

Tam, F., Churchill, N. W., Strother, S. C., & Graham, S. J. (2011). A new tablet for writing and drawing during functional MRI. *Human Brain Mapping*, *32*(2), 240-248.

Tsurugizawa, T., Taki, A., Zalesky, A., & Kasahara, K. (2023). Increased interhemispheric functional connectivity during non-dominant hand movement in right-handed subjects. *iScience*, *26*(9), 107592. https://doi.org/10.1016/j.isci.2023.107592

Tustison, N. J., Avants, B. B., Cook, P. A., Zheng, Y., Egan, A., Yushkevich, P. A., & Gee, J. C. (2010). N4ITK: improved N3 bias correction. *IEEE transactions on medical imaging*, *29*(6), 1310-1320.

Tzourio-Mazoyer, N., Petit, L., Zago, L., Crivello, F., Vinuesa, N., Joliot, M., Jobard, G., Mellet, E., & Mazoyer, B. (2015). Between-hand difference in ipsilateral deactivation is associated with hand lateralization: fMRI mapping of 284 volunteers balanced for handedness. *Front Hum Neurosci*, *9*, 5. https://doi.org/10.3389/fnhum.2015.00005

Valyear, K. F., & Frey, S. H. (2015). Human posterior parietal cortex mediates hand-specific planning. *NeuroImage*, *114*, 226-238. https://doi.org/10.1016/j.neuroimage.2015.03.058

van Kemenade, B. M., Arikan, B. E., Podranski, K., Steinstrater, O., Kircher, T., & Straube, B. (2019). Distinct Roles for the Cerebellum, Angular Gyrus, and Middle Temporal Gyrus in Action-Feedback Monitoring. *Cereb Cortex*, *29*(4), 1520-1531. https://doi.org/10.1093/cercor/bhy048

Vandierendonck, A. (2021). On the Utility of Integrated Speed-Accuracy Measures when Speed-Accuracy Trade-off is Present. *J Cogn*, *4*(1), 22. https://doi.org/10.5334/joc.154

Verstynen, T., Diedrichsen, J., Albert, N., Aparicio, P., & Ivry, R. B. (2005). Ipsilateral motor cortex activity during unimanual hand movements relates to task complexity. *J Neurophysiol*, *93*(3), 1209-1222. https://doi.org/10.1152/jn.00720.2004

Vingerhoets, G., Verhelst, H., Gerrits, R., Badcock, N., Bishop, D. V., Carey, D., Flindall, J., Grimshaw, G., Harris, L. J., & Hausmann, M. (2023). Laterality indices consensus initiative (LICI): A Delphi expert survey report on recommendations to record, assess, and report asymmetry in human behavioural and brain research. *Laterality*, *28*(2-3), 122-191.

Wang, J., & Sainburg, R. L. (2007). The dominant and nondominant arms are specialized for stabilizing different features of task performance. *Experimental brain research Experimentelle Hirnforschung Expérimentation cérébrale*, *178*(4), 565-570. https://doi.org/10.1007/s00221-007-0936-x

Wang, J., Tian, Y., Wang, M., Cao, L., Wu, H., Zhang, Y., Wang, K., & Jiang, T. (2016). A lateralized top-down network for visuospatial attention and neglect. *Brain Imaging Behav*, *10*(4), 1029-1037. https://doi.org/10.1007/s11682-015-9460-y

Waters-Metenier, S., Husain, M., Wiestler, T., & Diedrichsen, J. (2014). Bihemispheric Transcranial Direct Current Stimulation Enhances Effector-Independent Representations of Motor Synergy and Sequence Learning. *The Journal of Neuroscience*, *34*(3), 1037-1050. https://doi.org/10.1523/jneurosci.2282-13.2014

Wheaton, L., Fridman, E., Bohlhalter, S., Vorbach, S., & Hallett, M. (2009). Left parietal activation related to planning, executing and suppressing praxis hand movements. *Clinical Neurophysiology*, *120*(5), 980-986.

Wischnewski, M., Kowalski, G. M., Rink, F., Belagaje, S. R., Haut, M. W., Hobbs, G., & Buetefisch, C. M. (2016). Demand on skillfulness modulates interhemispheric inhibition of motor cortices. *Journal of Neurophysiology*, *115*(6), 2803-2813. https://doi.org/10.1152/jn.01076.2015

Wolpert, D. M., Goodbody, S. J., & Husain, M. (1998). Maintaining internal representations: the role of the human superior parietal lobe. *Nature neuroscience*, *1*(6), 529-533. http://www.nature.com/neuro/journal/v1/n6/abs/nn1098_529.html

Yang, Y., Li, J., Zhao, K., Tam, F., Graham, S. J., Xu, M., & Zhou, K. (2024). Lateralized Functional Connectivity of the Sensorimotor Cortex and its Variations During Complex Visuomotor Tasks. *The Journal of Neuroscience: the Official Journal of the Society for Neuroscience*, *44*(5). https://doi.org/10.1523/JNEUROSCI.0723-23.2023

Zhang, Y., Brady, M., & Smith, S. (2002). Segmentation of brain MR images through a hidden Markov random field model and the expectation-maximization algorithm. *IEEE transactions on medical imaging*, *20*(1), 45-57.